Polymer Chemistry

Accepted Manuscript

This is an *Accepted Manuscript*, which has been through the Royal Society of Chemistry peer review process and has been accepted for publication.

Accepted Manuscripts are published online shortly after acceptance, before technical editing, formatting and proof reading. Using this free service, authors can make their results available to the community, in citable form, before we publish the edited article. We will replace this *Accepted Manuscript* with the edited and formatted *Advance Article* as soon as it is available.

You can find more information about *Accepted Manuscripts* in the Information for Authors.

Please note that technical editing may introduce minor changes to the text and/or graphics, which may alter content. The journal's standard Terms & Conditions and the Ethical guidelines still apply. In no event shall the Royal Society of Chemistry be held responsible for any errors or omissions in this *Accepted Manuscript* or any consequences arising from the use of any information it contains.

ROYAL SOCIETY OF CHEMISTRY

www.rsc.org/polymers

Journal Name

RSCPublishing

ARTICLE

Regulation of self-assembly morphology of azobenzene-bearing double hydrophobic block copolymers in aqueous solution by shifting the dynamic host-guest complexation

Cite this: DOI: 10.1039/x0xx00000x

Received 00th January 2012,
Accepted 00th January 2012

DOI: 10.1039/x0xx00000x

www.rsc.org/

Zai-Zai Tong, Rui-Yang Wang, Jie Huang, Jun-Ting Xu,* Zhi-Qiang Fan

The double hydrophobic azobenzene-containing diblock copolymers, namely, poly(L-lactide)-*b*-poly[6-(4-(4-methoxyphenylazo)phenoxy)hexyl methacrylate] (PLLA-*b*-PMMAZO), were successfully prepared by sequential atom transfer radical polymerization (ATRP) and ring opening polymerization. These block copolymers (BCPs) can self-assemble into various morphologies in aqueous solution via host-guest interaction between the azobenzene (azo) groups and methyl-β-cyclodextrin (β-CD). The complexation equilibrium between azo and β-CD can be shifted by changing the length of hydrophobic PLLA block, micelle concentration or β-CD/azo molar ratio, thus the micellar morphology and size of the PLLA-*b*-PMMAZO/β-CD complexes are altered. A vesicle-to-sphere-to-entrapped vesicle transition was observed at β-CD/azo=1 as the PLLA block length increases. In addition, a large β-CD/azo ratio or higher micelle concentration leads to a vesicle-like morphology, while entrapped vesicles tend to be formed at a smaller β-CD/azo ratio or lower micelle concentration. It is found that prolongation of the UV irradiation time can also induce a vesicle-to-sphere-to-entrapped vesicle transition of the complex micellar morphology. Such a transition is reversible upon irradiation of visible light. In summary, the self-assembly behavior of PLLA-*b*-PMMAZO/β-CD complexes can be readily regulated by different methods. Moreover, the complexation between the azo groups and β-CD is inhomogeneous, which is responsible for the formation of entrapped vesicles and the microphase separation in the core of the spherical micelles and entrapped vesicles.

Introduction

In selective solvents, block copolymers (BCPs) can spontaneously self-assemble to form micelles of various structures, including sphere,[1-3] rod,[4-6] and vesicle[7,8], driven by the solvent-philic/solvent-phobic interactions of different blocks. The self-assembly morphology of BCPs in solution can be manipulated by altering the molecular parameters of BCPs (chemical structure, soluble-insoluble ratio and architectures of copolymers)[9-13] and external factors such as temperature, solvent quality and preparation method, etc.[13-17]

Nowadays, stimuli-responsive polymer micelles have captured considerable attention due to their potential applications in memory storage, biomedical materials, protein probes, and nano-devices.[18-21] Among numerous external stimuli, light is of special fascination because it can work in a most convenient way. It is found that azobenzene (azo) is especially advantageous to induce a dramatic structural change due to its photo-induced reversible *trans-cis* isomerization.[22-28] The change at the molecular level triggered by light can be amplified, leading to a change of the structure at a larger scale and the macroscopic properties. The photo-triggered self-assembly behaviors of azo-containing BCPs have been widely investigated.[29-39] Moreover, *trans*-azo is an excellent guest for inclusion complexation with β-cyclodextrin (β-CD) driven by hydrophobic and van der Waals interaction. In contrast, *cis*-azo cannot form an inclusion complex with β-CD due to the size mismatch between the host and guest.[40] Based on the host-guest recognition, the photoresponsive self-assembly of azo-bearing BCPs with cyclodextrin is well studied.[41-47]

However, one should bear in mind that the complexation between azo and β-CD is dynamic and there exist an equilibrium. Since the micelle solution of amphiphilic azo-bearing BCPs is usually prepared at a very low concentration, the complexation efficiency between azo units and β-CD may be small, though it is reported that the complexation constant between azo and β-CD is quite large (1700 M^{-1}).[48] Ji and Chen studied the effect of β-CD/azo ratio on the morphology transition of the amphiphilic BCPs and the

supramolecular assembly, respectively.[49,50] They found that not all β-CDs interacted with azo units when the ratio of β-CD/azo was 1. Only when more β-CD was introduced (β-CD/azo=5), all the β-CDs could interact with the azo-containing polymers and it led to a different morphology from that at a low β-CD/azo ratio. These results show that the inclusion complexation between azo and β-CD is inhomogeneous at a low concentration. Nevertheless, attention is rarely paid to the complexation equilibrium between azo and β-CD when studying self-assembly of azo-bearing BCPs. Because the complexed and un-complexed azo units have different hydrophilicity, the hydrophilic/hydrophobic ratio, which is a key factor determining the self-assembly morphology of BCPs, will be changed when the complexation equilibrium between azo and β-CD is shifted. As a result, it is expected that such an equilibrium can be utilized to regulate the self-assembly behavior of azo-bearing BCPs. Many factors, including micelle concentration, block length, molar ratio of β-CD/azo and light irradiation, can affect the complexation between azo and β-CD. From this viewpoint, controlled self-assembly of supramolecular amphiphiles can be readily realized, as compared with the conventional polymeric amphiphiles.

On the other hand, most of the researches on host-guest recognition-assisted assembly mainly focus on the amphiphilic azo-containing BCPs. Only recently Zhang reported that the spherical micelles of a double hydrophobic azo-containing BCP could dissociate and reassemble upon alternating irradiation of UV/visible light.[45] Study on the assembly behavior of double hydrophobic azo-containing BCPs with the aid of host-guest recognition is quite interesting and necessary, since it helps us understand the assembly behavior of BCPs in a broader range.

Herein, a series of azo-containing diblock copolymers, poly(L-lactide)-*b*-poly[6-(4-(4-methoxyphenylazo)phenoxy) hexyl methacrylate] (PLLA-*b*-PMMAZO), were prepared. These double hydrophobic BCPs can self-assemble into various micelles in aqueous solution after complexation with β-CD. Morphological transition of vesicle-to-sphere-to-entrapped vesicle can be readily achieved for the micelles of the complexes by different methods: the chain length of the PLLA block, micelle concentration, β-CD/azo molar ratio and light irradiation. Besides, microphase separation was observed in the core of the spherical micelles and entrapped vesicles, which was interpreted in terms of the inhomogeneous complexation between the azo groups and β-CD.

Experimental

Materials. Methyl-β-cyclodextrin (β-CD) was recrystallized from deionized water. L-lactide was purchased from Aldrich and recrystallized thrice from ethyl acetate and stored under nitrogen atmosphere prior to use. Tetrahydrofuran (THF) and toluene for polymerization were refluxed with sodium flakes and freshly distilled. Copper bromide was washed with acetic acid and diethyl ether for several times and dried under vacuum. Stanneous 2-ethylhexanoate ($Sn(Oct)_2$) (99%) was purchased from Acros and distilled under reduced pressure to remove the water prior to use. The other commercially available chemicals were used without further purification. The synthesis of 6-[4-(4-methoxyphenylazo)phenoxy]hexyl methacrylate (MMAZO) monomer was described in elsewhere.[51] The details for synthesis of initiator 2-hydroxyethyl 2-bromo-2-methylpro-panoate (2-HBMP) and the ^1H NMR spectrum of 2-HBMP are given in the supplementary information (Fig. S1).

Synthesis of PMMAZO. Atom transfer radical polymerization (ATRP) was chosen to prepare the azo-containing macroinitiator (PMMAZO). The detail synthesis of the PMMAZO is given as below. In a Schlenk flask, 1.24 g of MMAZO monomer, *N*,*N*,*N*′,*N*′,*N*″-pentamethyldiethylenetriamine (PMDETA) (30 μL), initiator 2-HBMP (8.8 μL), THF (10.0 mL) were mixed and stirred for 10 min. The mixture was immediately frozen in liquid nitrogen, and a vacuum was applied. After 3 freeze-thaw cycles, CuBr (9.0 mg) was added under N_2. Then the flask was put into an oil bath at 60 °C for 6 h. The product was dissolved in THF and passed through an alumina column to remove the metal complex. After being concentrated, the THF solution was precipitated in methanol. The purification by precipitation was repeated thrice and dried in a vacuum oven overnight at 40 °C.

Synthesis of PLLA-*b*-PMMAZO. A typical ring opening reaction for synthesis of diblock copolymer was described as follows in detail. PMMAZO macroinitiator, L-lactide were added into a Schlenk tube at predetermined molar ratio (Table1), sealed with a rubber septum, and repeatedly flashed with N_2 after evacuation. Freshly distilled toluene (2 mL/g L-lactide) was injected into the tube with a syringe, and then the tube was immersed in an oil bath with a temperature of 120 °C. Polymerization was initiated after 5 min by injecting a 10 wt% solution of the catalyst $Sn(Oct)_2$ in toluene corresponding to 0.1 mol% of the monomer. Polymerization was quenched after 24 h by cooling to room temperature. The polymer was precipitated in methanol thrice and died in a vacuum oven overnight at 40 °C.

Preparation of the micelle solutions. The micelle solutions were prepared by following Jiang's method.[52] The PLLA-*b*-PMMAZO diblock copolymer was first dissolved in THF to obtain a homogeneous solution with a concentration of 1 mg mL^{-1}, then 0.4 mL solution of PLLA-*b*-PMMAZO in THF was slowly injected into 4 mL solution of β-CD in water (β-CD/azo=1) at room temperature. The mixture solution was stirred for 30 min at 65 °C to evaporate the co-solvent THF and sonicated for 5 min to get the micelle solution. The final concentration of the micelle solution was 0.1 mg mL^{-1}.

Characterizations. Molecular weight and polydispersity index (PDI) were evaluated by gel permeation chromatography (GPC) using a Waters system calibrated with standard polystyrenes. THF was used

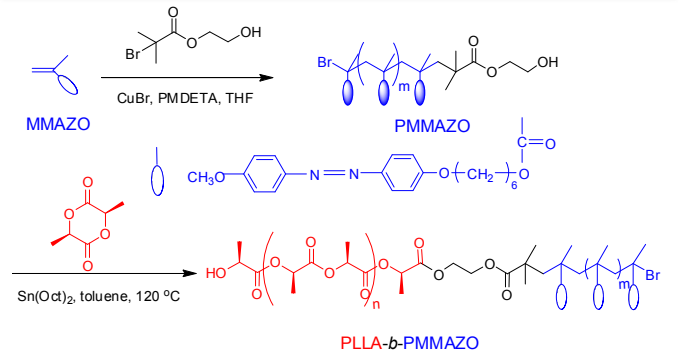

Scheme 1. The synthetic route of the PLLA-*b*-PMMAZO BCPs.

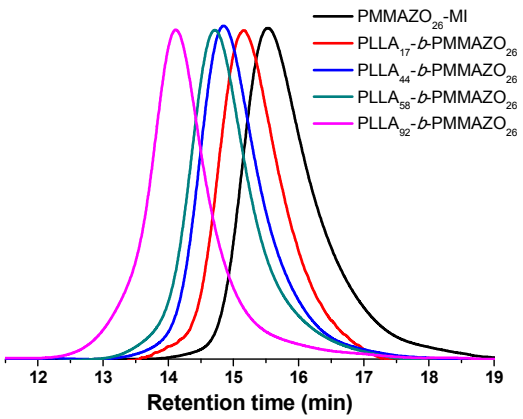

Fig. 1. GPC traces of PMMAZO homopolymer and PLLA-*b*-PMMAZO diblock copolymers with THF as the eluent.

as an eluent at a flow rate of 1.0 mL min^{-1}. ^{1}H NMR spectra were recorded on a Bruker DMX-400 MHz in $CDCl_3$ with tetramethylsilane (TMS) as an internal reference. Fluorescence spectra were measured on a Thermo Scientific Lumina Fluorescence Spectrometer. The UV-Vis spectra of the samples were measured over different irradiation time intervals on a Cary 100 UV-Vis spectrometer. Dynamic light scattering (DLS) measurements were carried out on a Brookhaven Instrument BI-200SM with a laser wavelength of 636 nm at 25 °C at a scattering angle of 90°. The data were analyzed with the software supplied by Brookhaven. TEM observations were carried out on a JEOL JEM-1230 electron microscope at an acceleration voltage of 80 kV. TEM samples were prepared by dropping 4 μL of the micellar solution onto carbon-coated copper grids, then the samples were frozen by liquid nitrogen and freeze-dried under the vacuum to avoid any possible reassembly and aggregation of the micelles during the drying process. Parts of the samples were negatively stained with phosphotungstic acid (PTA) aqueous solution for 10 min after drying for better clarity. Irradiation of the samples with UV light (365 nm) was performed with a UV-lamp (45 mW cm^{-2}) and the distance between the UV-lamp and the sample is about 50 cm.

Results and Discussion

Synthesis of azo-bearing diblock copolymers. The azo-bearing diblock copolymers (PLLA-*b*-PMMAZO) were synthesized via ATRP and ring opening polymerization as shown in Scheme 1. The PMMAZO homopolymer and a series of PLLA-*b*-PMMAZO BCPs with narrow polydispersity (PDI<1.14) were successfully prepared, which is confirmed by the GPC and ^{1}H NMR. Fig. 1 shows the GPC traces of the PMMAZO homopolymer and four PLLA-*b*-PMMAZO

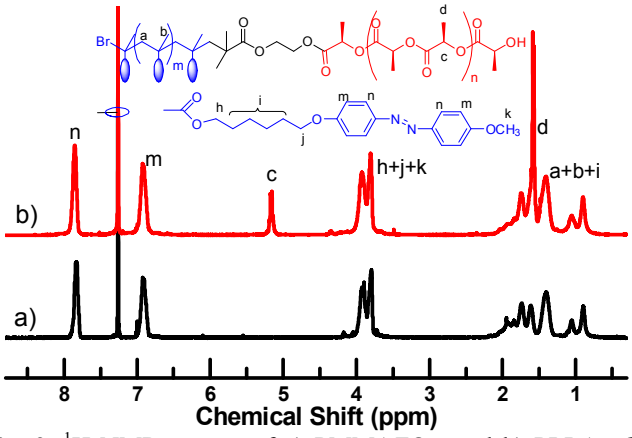

Fig. 2. ^{1}H NMR spectra of a) $PMMAZO_{26}$ and b) $PLLA_{17}$-*b*-$PMMAZO_{26}$ diblock copolymer in $CDCl_3$.

BCPs. It can be seen that the molecular weights of block copolymers increased with the molar ratio of the LLA monomer to macroinitiator (M/I in the Table 1). The composition of four BCPs can be further calculated from the ^{1}H NMR result. Fig. 2 shows the representative ^{1}H NMR spectra of PMMAZO and $PLLA_{17}$-*b*-$PMMAZO_{26}$ in $CDCl_3$. One can see that newly emerging signals (*c* and *d*) are assigned to the PLLA block, which indicates the diblock copolymer is successfully synthesized. From the area ratio of the ^{1}H NMR peaks corresponding to the PMMAZO (signal *n*) and PLLA blocks (signal *c*), the composition of the BCPs can be calculated. The polymerization result of four PLLA-*b*-PMMAZO BCPs with weight fraction of the PLLA block varying from 0.19 to 0.56 is included in Table 1.

Self-assembly of the PLLA-*b*-PMMAZO/β-CD complexes in water

Critical micellization concentrations of the complexes. It is well known that the morphologies and sizes of self-assemblies from an amphiphilic block copolymer in aqueous solution are mainly determined by the block length, and the hydrophilic/hydrophobic ratio. For the PLLA-*b*-PMMAZO block copolymers, both blocks are hydrophobic and thus they cannot form micelles in water. However, the azo-containing PMMAZO block can interact with β-CD by host-guest inclusion complexation. The PMMAZO/β-CD complex is water-soluble and thus the PLLA-*b*-PMMAZO/β-CD can self-assemble in water. Before studying the self-assembly behavior of the PLLA-*b*-PMMAZO/β-CD complexes, the critical micellization concentrations (CMCs) of the complexes should be known. The CMCs of the amphiphilic complexes were determined by using pyrene as a fluorescent probe. After micellization, the pyrene

Table 1. Molecular characteristics of PMMZAO homopolymer and diblock copolymers.

Run	M/I[a)]	Conv (NMR)	M_n^{GPC}	PDI^{GPC}	Composition (NMR)	M_n^{NMR}	W_{PLLA}
0	50	49% [b)]	10400	1.11	$PMMAZO_{26}$ [c)]	-	0
1	20	85%	13300	1.10	$PLLA_{17}$-*b*-$PMMAZO_{26}$	12700	0.19
2	50	88%	15900	1.11	$PLLA_{44}$-*b*-$PMMAZO_{26}$	16600	0.38
3	60	97%	16700	1.14	$PLLA_{58}$-*b*-$PMMAZO_{26}$	18600	0.45
4	100	92%	25600	1.13	$PLLA_{92}$-*b*-$PMMAZO_{26}$	23500	0.56

[a] Molar ratio of monomer to initiator; [b] based on mass yield; [c] Using GPC-determined block.

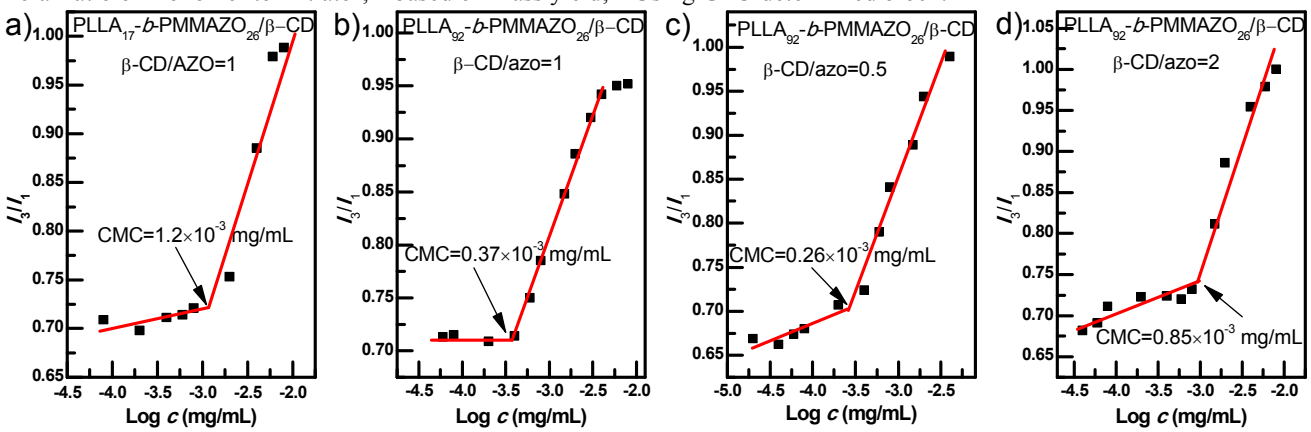

Fig. 3. Effect of concentration on the fluorescence intensity ratio I_3/I_1 from pyrene excitation spectra: a) $PLLA_{17}$-b-$PMMAZO_{26}$/β-CD at β-CD/azo=1 and b) $PLLA_{92}$-*b*-$PMMAZO_{26}$/β-CD at β-CD/azo=1; c) $PLLA_{92}$-*b*-$PMMAZO_{26}$/β-CD at β-CD/azo=0.5 and d) $PLLA_{92}$-*b*-$PMMAZO_{26}$/β-CD at β-CD/azo=2.

probe will be preferentially located in the hydrophobic domains of micelles,[53] leading to a rapid rise in the intensity ratio of the peaks at 383 and 371 nm (I_3/I_1) of pyrene in the excitation spectra.[45] As shown in Fig. 3, the CMC of $PLLA_{17}$-*b*-$PMMAZO_{26}$/β-CD (β-CD/azo=1) is determined to be 1.2×10^{-3} mg mL^{-1}. By contrast, it is 0.37×10^{-3} mg mL^{-1} for $PLLA_{92}$-*b*-$PMMAZO_{26}$/β-CD (β-CD/azo=1). This is quite normal, since a larger hydrophilic/ hydrophobic ratio will increase the CMC of BCPs. The effect of β-CD/azo ratio on CMC of $PLLA_{92}$-*b*-$PMMAZO_{26}$/β-CD was also studied. The CMCs are 0.26×10^{-3} and 0.85×10^{-3} mg mL^{-1} for β-CD/azo=0.5 and 2, respectively. This indicates that the β-CD/azo ratio can affect the stability of PLLA-*b*-PMMAZO/β-CD complexes. More azo units are complexed at a larger β-CD/azo ratio, leading to a larger hydrophilic/hydrophobic ratio and thus a higher CMC.

Effect of PLLA block length. After knowing the CMCs of the complexes, we firstly examined the self-assembly behavior of the complexes of four BCPs with β-CD in aqueous solution with a molar ratio of β-CD/azo=1. The micelle concentration is fixed at 0.1 mg mL^{-1}, which is similar to that used in literature and well above the CMCs of the complexes. The size distribution obtained from DLS and morphologies captured by TEM are shown in Fig. 4. One can see that the aggregation size of the PLLA-*b*-PMMAZO/β-CD complexes varies with the chain length of the PLLA block. With increasing the PLLA block length, the particle size of the aggregates increases as well. TEM reveals that the $PLLA_{17}$-*b*-$PMMAZO_{26}$/β-CD complex, in which the PLLA block is the shortest, forms vesicle-like micelles with a diameter ranging from 40-100 nm and a wall thickness about 10 nm. We notice that the size of the vesicles measured by TEM is smaller than that obtained by DLS. This difference may be due to the swelling of the soluble corona in the solution.

When the PLLA block becomes longer, the micelles of the $PLLA_{44}$-*b*-$PMMAZO_{26}$/β-CD complex have an irregular spherical shape with a stripe structure (Fig. 4c). It should be noted that the micelles in Fig. 4c were stained with PTA. Since the PLLA block cannot be stained by PTA,[54] the bright stripe phase should be the domain of PLLA. As compared with the vesicular micelles of $PLLA_{17}$-*b*-$PMMAZO_{26}$/β-CD, it is quite strange that $PLLA_{44}$-*b*-$PMMAZO_{26}$/β-CD with a longer hydrophobic PLLA block forms spherical micelles. According to Eisenberg's theory,[7] the BCP with a lower fraction of hydrophilic block tends to form vesicular micelles, while the BCP with a higher fraction of hydrophilic block prefers to self-assemble into star-like spherical micelles. Herein, we believe that the micelles of $PLLA_{44}$-*b*-$PMMAZO_{26}$/β-CD in Fig. 4c are crew-cut, in which the corona is relatively short.

In order to quantitatively describe the impact of PLLA block length on the self-assembly morphology evolution, the complexation efficiency (CE), which is defined as the fraction of complexed azo moiety, was calculated in terms of the complexation constant between β-CD and azo (1700 M^{-1} in aqueous solution[48]):

$$CE = \frac{\frac{1}{1700} + (1+r)\frac{26c}{M_n^{BCP}} - \sqrt{[\frac{1}{1700} + (1+r)\frac{26c}{M_n^{BCP}}]^2 - 4r(\frac{26c}{M_n^{BCP}})^2}}{2\times\frac{26c}{M_n^{BCP}}} \quad (1)$$

Where r is the molar ratio of β-CD/azo, M_n^{BCP} is the molecular weight of a BCP obtained from NMR and c is the micelle concentration. The calculated result is summarized in Table 2. One can see that the CE is only 0.215 for $PLLA_{17}$-*b*-$PMMAZO_{26}$/β-CD, and it is reduced to 0.182 when the polymerization degree of the PLLA block is 44. This shows that there exist lots of uncomplexed azo groups, which makes the PMMAZO block similar to a random amphiphilic copolymer. As a result, parts of the uncomplexed or less complexed PMMAZO segments may also aggregate into the core of the spherical micelles. The evidence lies in that the inner core of the micelles is composed of the periodical grey and white stripes, which possibly results from the microphase separation between the incompatible uncomplexed or less complexed PMMAZO and PLLA. After being stained with PTA, the inner structure of the core can be clearly observed (Fig. 4c and Fig. S2b of supplementary information), as compared with the un-stained micelles (Fig. S2a of supplementary information). The hydrophilic ratio (f_{philic}), i.e. the

weight fraction of the hydrophilic segments, can be calculated based on following equation.

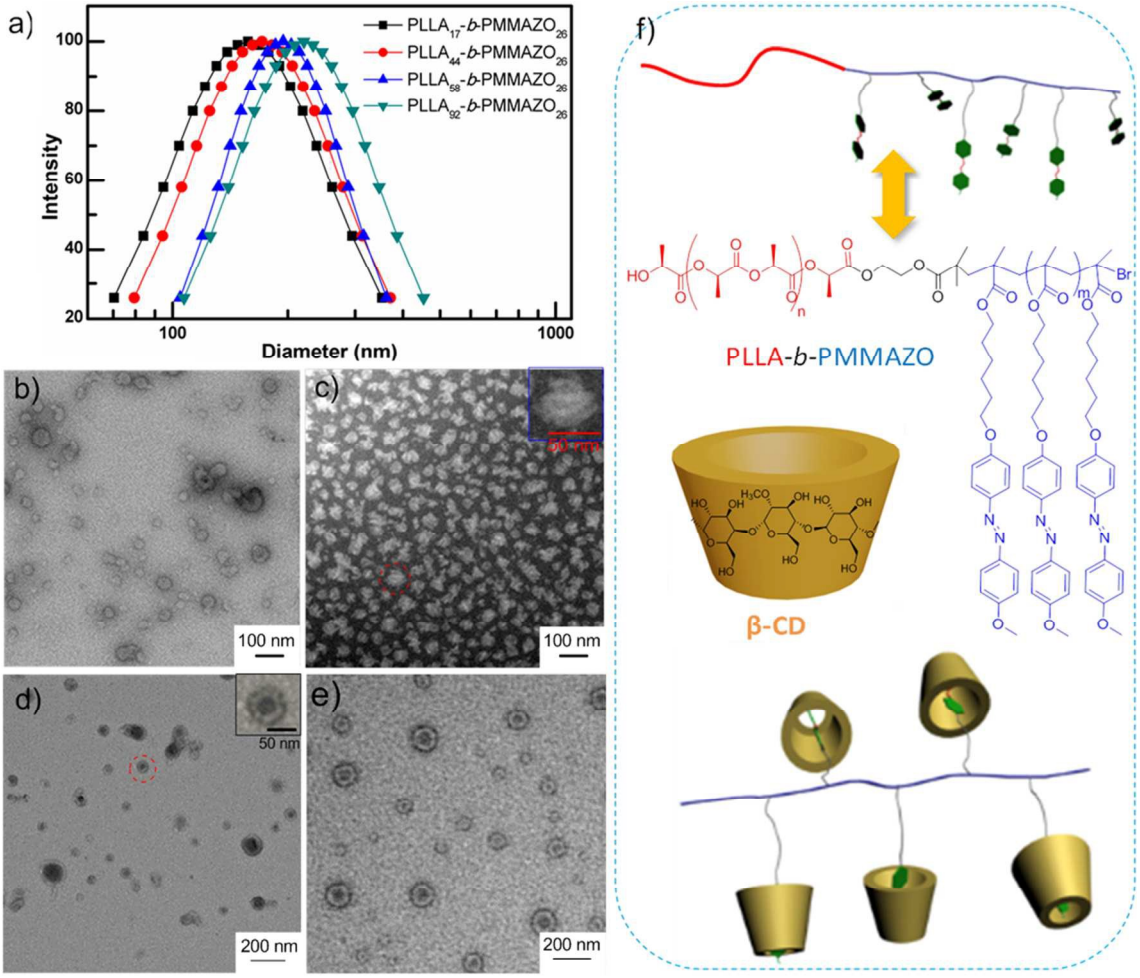

Fig. 4. a) Size distributions of four PLLA-*b*-PMMAZO/β-CD complexes (β-CD/azo=1) in aqueous solution (c=0.1 mg mL^{-1}). TEM images of the PLLA-*b*-PMMAZO/β-CD complexes (β-CD/azo=1) in aqueous solution (c=0.1 mg mL^{-1}). b) $PLLA_{17}$-*b*-$PMMAZO_{26}$, c) $PLLA_{44}$-*b*-$PMMAZO_{26}$, d) $PLLA_{58}$-*b*-$PMMAZO_{26}$ and e) $PLLA_{92}$-*b*-$PMMAZO_{26}$, inset is the detail structure of micelle in the corresponding red dash circle. Sample in c) was stained with PTA for 10 min. f) Illustration of the inclusion complexation between the azo group and β-CD.

$$f_{philic} = \frac{26CE(M^{AZO} + M^{\beta-CD})}{(M_n^{BCP} + 26CE \times M^{\beta-CD})} \qquad (2)$$

Where M^{AZO} is the molecular weight of azo moiety (M^{AZO} =211), $M^{\beta\text{-CD}}$ is the molecular weight of β-CD ($M^{\beta\text{-CD}}$=1303). It is found that vesicles are formed at f_{philic}=0.423, while spheres are fabricated at 0.314 (Table 2). Li also observed vesicles (or polymersomes) at a f_{philic} around 0.4 in amphiphilic BCPs containing a liquid crystalline block,[55] which is very similar to our result. In addition, since spheres are formed at a smaller f_{philic}, it is reasonable that the $PLLA_{44}$-*b*-$PMMAZO_{26}$/β-CD complex forms crew-cut micelles at β-CD/azo=1.

When the polymerization degree of PLLA is increased to 58 and 92, the CEs become further smaller, and the values of f_{philic} are also decreased to 0.280 and 0.194, respectively. As a consequence, the self-assembly morphology of the complexes changes accordingly. One can see that $PLLA_{58}$-*b*-$PMMAZO_{26}$/β-CD forms the mixture of spheres and vesicles with a spherical particle entrapped inside (Fig. 4d). There exists a domain (bright phase, Fig. 4d) between the core and wall of the vesicles. Such self-assembly morphology is called as entrapped vesicle, which is rarely reported for block copolymer micelles.[56,57] The formation mechanism of the entrapped vesicle will be discussed in the following section. As shown in Fig. 4d (inset), the overall size of a typical entrapped vesicle is about 70 nm, and the wall thickness of the vesicular layer is about 10 nm (inset in Fig. 4d). The size of the spherical particle entrapped inside the vesicle is about 30 nm, and the gap between wall of the vesicle and sphere is also about 10 nm. As compared with self-assembly morphology of the $PLLA_{58}$-*b*-$PMMAZO_{26}$ complex, uniform entrapped vesicles with a larger size are observed for the $PLLA_{92}$-*b*-$PMMAZO_{26}$/β-CD complex.

Effect of micelle concentration. Above result reveals that the self-assembly morphology of the PLLA-*b*-PMMAZO/β-CD complexes

at β-CD/azo=1 in aqueous solution changes with the hydrophilic/hydrophobic ratio. Due to the low concentration of the micelle solution (0.1 mg mL^{-1}), the CE of the azo group is rather small. Since the CE is dependent on both the concentrations of β-CD and azo moiety, if we increase the micelle concentration or the β-CD/azo ratio, the hydrophilic/hydrophobic ratio and the self-assembly morphology may be altered accordingly. We prepared the micelle solutions of PLLA$_{92}$-*b*-PMMAZO$_{26}$/β-CD complex at various concentrations. The calculated values of CE and f_{philic} are summarized in Table 2. The size and morphology at different concentrations are shown in Fig. 5. One can see that the f_{philic} varies from 0.194 to 0.458 when the micelle concentration changes from 0.1 to 0.8 mg mL^{-1}. At the same time, the size of the micelles is increased from 222 nm at *c*=0.1 mg mL^{-1} to 280 nm at *c*=0.8 mg mL^{-1}. If we dilute the micelle solution from 0.8 mg mL^{-1} to 0.1 mg mL^{-1}, the effective diameter of the micelles is reduced to 212 nm, which is very similar to the size of the micelles directly prepared at 0.1 mg mL^{-1}.

Table 2. Effects of PLLA length, micelle concentration and β-CD/azo ratio on the complexation efficiency between azo and β-CD/azo and the hydrophilic ratio of the complexes.

Sample name	Concentration (mg mL^{-1})	β-CD/azo	Complexed azo (CE)	Complexed β-CD	Free β-CD	f_{philic}	Morphology
PLLA$_{17}$-*b*-PMMAZO$_{26}$	0.1	1	21.5%	21.5%	78.5%	0.423	vesicle
PLLA$_{44}$-*b*-PMMAZO$_{26}$	0.1	0.5	10.3%	20.6%	70.4%	0.202	entrapped vesicle
	0.1	1	18.2%	18.2%	81.8%	0.314	sphere
	0.1	2	32.3%	16.2%	83.8%	0.461	vesicle
PLLA$_{58}$-*b*-PMMAZO$_{26}$	0.1	1	17.5%	17.5%	82.5%	0.280	entrapped vesicle, sphere
PLLA$_{92}$-*b*-PMMAZO$_{26}$	0.1	1	13.9%	13.9%	86.1%	0.194	entrapped vesicle
	0.2	1	22.3%	22.3%	77.7%	0.288	sphere
	0.4	1	32.7%	32.7%	67.3%	0.372	vesicle
	0.8	1	45.2%	45.2%	54.8%	0.458	Large compound micelles

As we can see, PLLA$_{92}$-*b*-PMMAZO$_{26}$/β-CD forms entrapped vesicles at *c*=0.1 mg mL^{-1} (Fig. 4e). When the micelle concentration is increased from 0.2 to 0.8 mg mL^{-1}, the micellar morphology changes from sphere to vesicle, and then to large compound micelle. Similarly, if we dilute the micelle solution with a concentration of 0.8 mg mL^{-1} to 0.1 mg mL^{-1}, entrapped vesicles are reconstructed, as shown in Fig. 5e. This result indicates that the inclusion complexation between azo group and β-CD is dynamically equilibrated in aqueous solution, and such an equilibrium shifts quickly as the concentration changes. The transition of the self-assembly morphology with micelle concentration can also be attributed to the different hydrophilic/hydrophobic ratios at various concentrations. This shows that, increase of micelle concentration and decrease of the PLLA block length have a similar effect on the self-assembly morphology of the PLLA-*b*-PMMAZO/β-CD complexes to some extent.

Effect of β-CD/azo ratio. On the other hand, when we change the β-CD/azo ratio, the CE of the azo group and thus the hydrophilic/hydrophobic ratio will be altered as well. Therefore, we believe the self-assembly morphology of the PLLA-*b*-PMMAZO/β-CD complexes can also be regulated by the β-CD/azo ratio. We studied the self-assembly morphology of PLLA$_{44}$-*b*-PMMAZO$_{26}$/β-CD complexes at β-CD/azo=0.5, 1 and 2, respectively. The micelle concentrations were kept the same (0.1 mg mL^{-1}). The calculated values of CE and f_{philic} are listed in Table 2. It is observed that, the

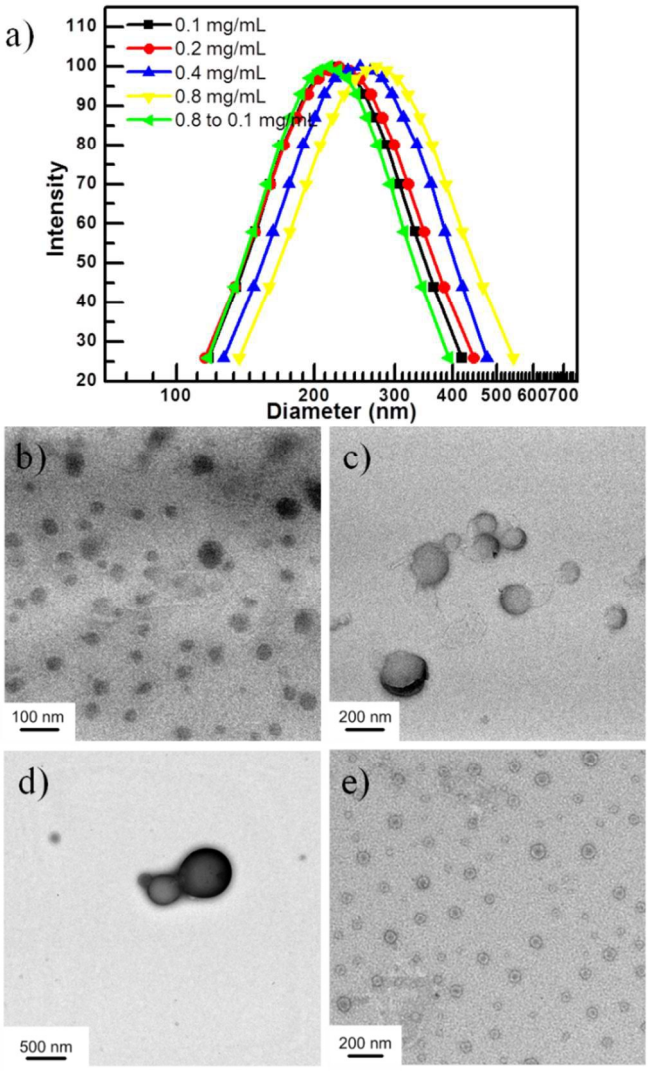

Fig. 5. Effect of micelle concentration on the micellar size and morphology evolution of PLLA$_{92}$-*b*-PMMAZO$_{26}$/β-CD complex. a) Size distribution at various micelle concentrations; b) TEM images

for the micelles of PLLA$_{92}$-*b*-PMMAZO$_{26}$/β-CD complex at *c*=0.2 mg mL^{-1}; c) at *c*=0.4 mg mL^{-1}; d) at *c*=0.8 mg mL^{-1}; and e) at 0.1 mg mL^{-1} diluted from 0.8 mg mL^{-1}.

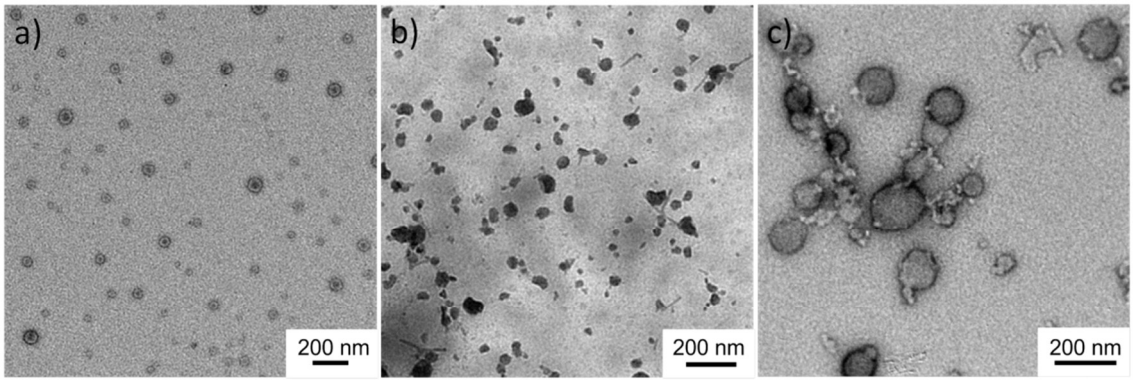

Fig. 6. Effect of β-CD/azo ratio on the micellar morphology of PLLA$_{44}$-*b*-PMMAZO$_{26}$ complexes (*c*=0.1 mg mL^{-1}): a) 0.5:1; b) 1:1 and c) 2:1.

CE increases from 10.3% to 32.3% and the f_{philic} changes from 0.202 to 0.461, as the β-CD/azo ratio varies from 0.5 to 2. Fig. 6 shows the TEM images of the PLLA$_{44}$-*b*-PMMAZO$_{26}$/β-CD micelles at various β-CD/azo ratios. As we can see, uniform entrapped vesicles are formed at β-CD/azo=0.5, while spherical micelles are observed at β-CD/azo=1. When the β-CD/azo ratio is increased to 2, the micellar morphology is completely changed into vesicle. As a result, increase of the β-CD/azo ratio can induce the entrapped vesicle-to-sphere-to-vesicle transition of the micellar morphology of PLLA$_{44}$-*b*-PMMAZO$_{26}$/β-CD complex. The TEM images of the self-assembly morphology of PLLA$_{92}$-*b*-PMMAZO$_{26}$/β-CD complexes at various β-CD/azo ratios are supplied in Fig. S3 of supplementary information. It is observed that the micellar morphology of PLLA$_{92}$-*b*-PMMAZO$_{26}$/β-CD changes with the β-CD/azo ratio in a way similar to the PLLA$_{44}$-*b*-PMMAZO$_{26}$/β-CD complex. This result further confirms that the entrapped vesicle is formed due to the smaller hydrophilic/hydrophobic ratio, since the PMMAZO block is less hydrophilic at a smaller β-CD/azo ratio.

The interaction between the azo groups and β-CD at various β-CD/azo ratios can further be experimentally identified by ^{1}H NMR. The chemical shift of the -OCH$_3$ proton of β-CD located at the inner surface of the cavity was compared with that of the proton in the residual THF reference (1.88 ppm). It is noted that, during preparation of the micelle solution, the PLLA-*b*-PMMAZO was first dissolved in THF and the THF solution was added into the aqueous solution of β-CD. It seems difficult to completely remove THF from the micelle solution even after vigorously stirring around the boiling temperature of THF (65 °C) for a long time. However, the concentration of the residual THF in micelle solution estimated from the NMR is only about 0.3 wt%, thus the effect of the residual THF on the micellar morphology is ignored. The ^{1}H NMR spectra of uncomplexed β-CD and β-CD in the D$_2$O solution of PLLA$_{92}$-*b*-PMMAZO$_{26}$/β-CD complexes at various β-CD/azo ratios are shown in Fig. 7. It is observed that the two protons of uncomplexed β-CD are located at 5.22 ppm and 5.02 ppm, respectively. By contrast, for the resonances of the complexed protons at various β-CD/azo ratios, a prominent upfield shift is detected, although the fraction of free β-CD is dominated. Moreover, as the β-CD/azo ratio decreases, a larger shift to upfield position occurs and the difference in the chemical shift between the complexed and uncomplexed β-CD becomes smaller. This shows that, with increasing the β-CD/azo ratio, the fraction of uncomplexed β-CD is higher. Such a result is consistent with the variation of the calculated CE (Table 2) and the morphology evolution (Fig. 6) with the β-CD/azo ratio.

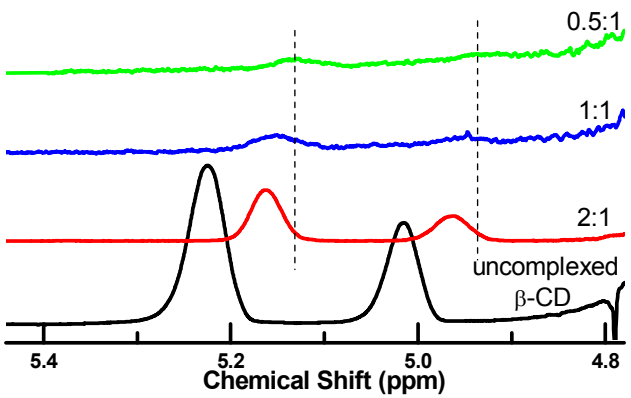

Fig. 7. ^{1}H NMR spectra of the uncomplexed β-CD, and β-CD in the PLLA$_{92}$-*b*-PMMAZO$_{26}$/β-CD complex in D$_2$O at various β-CD/azo ratios.

Micellar structures of the PLLA-*b*-PMMAZO/β-CD complexes

We can see from above results that, the self-assembly morphology of PLLA-*b*-PMMAZO/β-CD complexes varies with the PLLA block length, micelle concentration and β-CD/azo ratio, as illustrated in Scheme 2. Generally, the effects of above parameters can be attributed to the change of the key parameter, f_{philic}, as shown in Table 2. When f_{philic} is larger than 0.372, vesicles tend to be formed. By contrast, spheres are formed when f_{philic} ranges from 0.288 to 0.314. If f_{philic} is further decreased to 0.202, entrapped vesicles are preferentially produced.

We notice that the CEs of the azo groups under various conditions are rather low. Moreover, the complexation between azo and β-CD is random and dynamic. Consequently, the complexed

PMMAZO blocks are quite inhomogeneous, i.e. there exist both less and more complexed PMMAZO blocks. The inhomogeneous PMMAZO blocks may result in some particular structures of the micelles of the PLLA-*b*-PMMAZO/β-CD complexes. For the spherical micelles, the core is composed of the less complexed PMMAZO block and the PLLA block. The incompatibility between

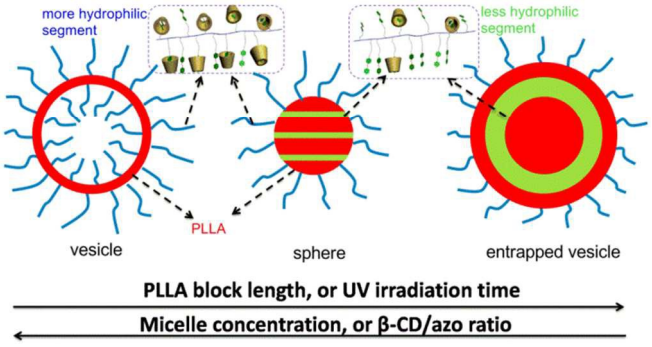

Scheme 2. Illustration for the structures of three micellar morphologies of PLLA-*b*-PMMAZO/β-CD complexes in aqueous solution and regulation of the micellar morphology by different methods.

them leads to a lamellar microphase-separated structure of the micellar core. It should be noted that the microphase separation takes place in nano-spheres, which is like a BCP confined in spherical domains. Under such a spatially confined environment, formation of a lamellar microphase-separated structure is usually due to the large ratio of the particle size over the lamellar *d*-spacing of the BCPs.[58]

There exists microphase separation inside the entrapped vesicles as well. As schematically depicted in Scheme 2, the entrapped core and wall of the vesicles (dark domains in Fig. 4d) are composed of PLLA, and the bright domain between the entrapped core and wall of the vesicles corresponds to the PMMAZO blocks complexed with a smaller fraction of β-CD. The outside of the vesicle wall is the PMMAZO blocks complexed with a larger fraction of β-CD, which are more hydrophilic but cannot be observed by TEM. It should be pointed out that the microphase-separated structure inside the entrapped vesicles is a spherical PLLA core wrapped by a concentric layer of less complexed PMMAZO, which is different from the alternate lamellar structure in the core of the spherical micelles. Formation of such a microphase-separated structure is possibly due to the asymmetric vesicle structure in the entrapped vesicles. The outside of the vesicle wall is more complexed PMMMAZO, but the inner-side is less complexed PMMAZO, which will be more affinitive to the chemically linked PLLA core. The selective affinity of the inner surface of the hollow sphere toward one of the blocks usually leads to formation of a concentric layered structure of microphase separation for BCPs confined in spherical domains.[58]

Generally, micelles with a microphase-separated core are observed for ABC triblock terpolymers, in which one of the blocks is solvent-soluble and forms the micellar corona, but the remaining two blocks are both solvent-phobic and form the micellar core. However, since the core-forming two blocks are immiscible, microphase separation occurs in the micellar core.[59-64] In the present work, the micellar core is the less complexed PLLA-*b*-PMMAZO (in the entrapped vesicles) or the mixture of the less complexed PLLA-*b*-PMMAZO and the PLLA block connected with more complexed PMMAZO block (in the spherical micelles). Therefore, microphase separation may also take place in the micellar core. The difference between the micelles of PLLA-*b*-PMMAZO/β-CD complexes and common ABC triblock BCPs lies in that the micellar core is not or only partially connected with the micellar corona. As a result, the origin for occurrence of microphase separation in the micellar core of PLLA-*b*-PMMAZO/β-CD complexes is the inhomogeneous complexation between the azo groups with β-CD. The less complexed PMMAZO blocks are also incorporated into the micellar core, which will segregate from the hydrophobic PLLA block. The inhomogeneous complexation between the azo groups and β-CD may be also responsible for the formation of the entrapped vesicles. Because of the co-existence of the more and less complexed PLLA-*b*-PMMAZO, the less complexed PLLA-*b*-PMMAZO is unstable in the aqueous solution and tends to be wrapped by the vesicles formed by the more complexed PLLA-*b*-PMMAZO.

We wonder whether the entrapped vesicle is the result of kinetic trap or is metastable. The solutions of the $PLLA_{92}$-*b*-$PMMAZO_{26}$/β-CD and $PLLA_{44}$-*b*-$PMMAZO_{26}$/β-CD containing entrapped vesicles or phase separated spheres were annealed at the temperature around the glass transition temperature of the PLLA block (65 °C) for 24 h. It is found that the size and morphology of the micelles are almost the same as un-annealed micelles (Fig. S4 in supplementary information). This shows that the entrapped vesicles are thermodynamically stable in aqueous solution. The sphere-to-entrapped vesicle transition resulting from dilution of the micellar solution (Fig. 5) also confirms that formation of the entrapped vesicles is not the result of kinetic trap.

The entrapped vesicles may have potential applications in highly efficient dispersion of hydrophobic materials and controlled drug delivery. As a result, it is important to understand the formation mechanism of entrapped vesicle. The entrapped vesicles were first observed by Petrov in the aqueous solution of poly(ethylene oxide)-*block*-poly(n-butyl acrylate) (PEO_{113}-*b*-$PnBA_{243}$),[56] but they didn't propose a mechanism for the formation of entrapped vesicles. Salim also observed this intriguing morphology for the poly(ethylene oxide)-*block*-poly(lactide) (PEO-*b*-PLA)/poly(acrylic acid) (PAA) complexes with a molar ratio of EO:AA=1 in the H_2O/THF mixed solvent.[57] They believed that this morphology was the result of the increased free energy reflecting the stretching of the core-forming PLA block and the change of the interaction among different PEO blocks caused by complexation with PAA. As for the formation pathway, they proposed that the formation of entrapped vesicles started from the large vesicles at a high polymer concentration and a high water content. Nevertheless, the heterogeneity of the complexation between PAA and PEO was not discussed. Here in our system, the inhomogeneous complexation between azo and β-CD may be the main factor for the fabrication of the entrapped vesicles. Moreover, the structure of the entrapped vesicles is kinetically frozen after addition of selective solvent in literature.[56,57] By contrast, the micelles of PLLA-*b*-PMMAZO/β-CD complexes are thermodynamically equilibrated, since the micellar morphology changes quickly with dilution of the micelle solution (Fig.5e).

Photo-regulated self-assembly of the PLLA-*b*-PMMAZO/β-CD complexes

It is well known that *trans*-azo isomer has a strong binding affinity with β-CD in aqueous solution, while the binding force between the *cis*-azo isomer and β-CD is weak. On the other hand, the reversible *trans-cis* isomerization of the azo groups can be readily realized

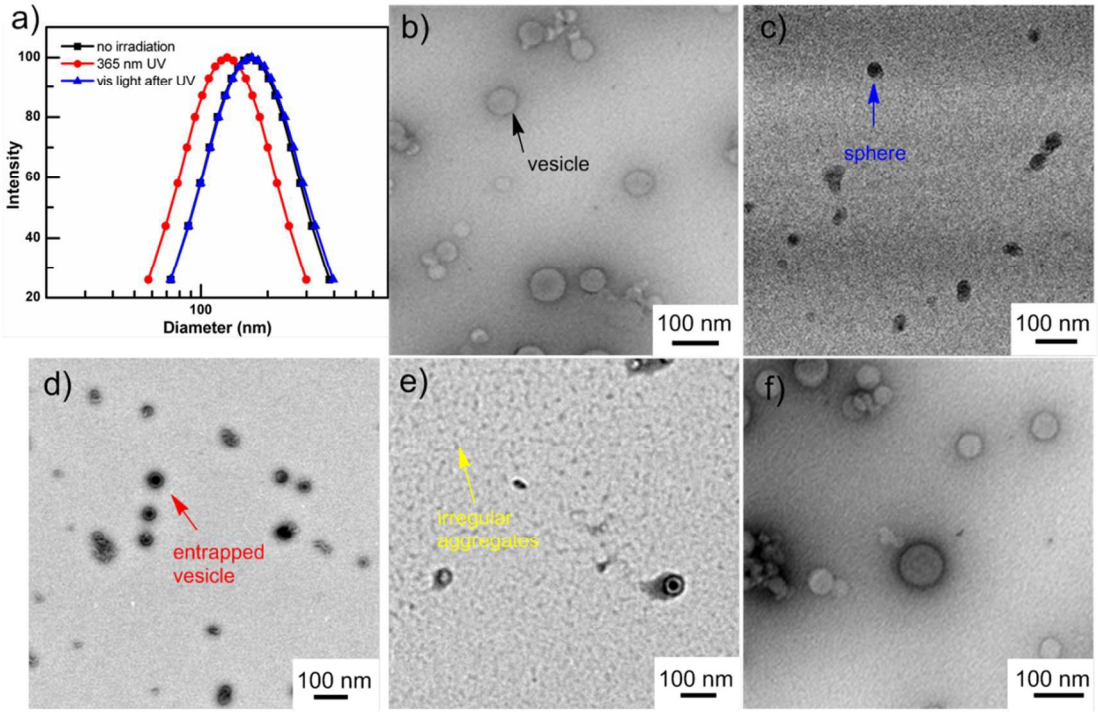

Fig. 8. a) Size distribution of the $PLLA_{17}$-*b*-$PMMAZO_{26}$/β-CD complex at β-CD/azo=1 before (black) and after (red) UV irradiation, and after subsequent irradiation with visible light (blue). The TEM images of the complex micelles. b) before UV irradiation; c) after UV irradiation for 1 min; d) for 3 min; e) for 30 min and f) after subsequent irradiation with visible light for 30 min.

upon irradiation of light with different wavelengths. This indicates that the inclusion complexation between β-CD and azo is reversible as the photo-isomerization of azobenzene occurs. Based on this result, it is expected that regulation of the self-assembly morphology of the PLLA-*b*-PMMAZO/β-CD complexes may be achieved via change of light irradiation time. It should be pointed out that, although the *trans-cis* isomerization at the molecular level is very fast (see Fig. S5 in supplementary information), the transition of the self-assembly morphology at a large scale may be relatively slower, since we didn't observe morphological change for the micelles of $PLLA_{17}$-*b*-$PMMAZO_{26}$/β-CD complex after UV irradiation for 30 s. However, prolongation of UV irradiation time can trigger the morphological transition of the micelles. Fig. 8 represents the micellar size and morphology of the $PLLA_{17}$-*b*-$PMMAZO_{26}$/β-CD complex at β-CD/azo=1 before and after UV irradiation for various times, then further irradiated with visible light. One can see that before UV irradiation, the $PLLA_{17}$-*b*-$PMMAZO_{26}$/β-CD forms vesicles in aqueous solution (Fig. 8b). After irradiation of 365 nm UV for 1 min, the micellar morphology transforms into sphere (Fig. 8c). Entrapped vesicles are observed at further increased irradiation time (3 min), as shown in Fig. 8d. Therefore, as the UV irradiation time increases, the vesicle-to-sphere-to-entrapped vesicle transition can be realized for the micelles of the $PLLA_{17}$-*b*-$PMMAZO_{26}$/β-CD complex. Such a transition can be ascribed to the gradual decrease of the fraction of the *trans*-azo isomer and the hydrophilic/hydrophobic ratio in the complex with increasing UV irradiation time. In the previous section, we pointed out that a larger f_{philic} is favourable to formation of vesicles, whereas entrapped vesicles tend to be formed at a smaller f_{philic}. Herein we find that UV irradiation has an equivalent effect with increasing the PLLA length or lowering the micelle concentration and β-CD/azo ratio, as illustrated in Scheme 2. We also try to evaluate the f_{philic} at different UV irradiation times, since the fraction of *trans*-azo moieties has a linear relationship with UV irradiation time (Fig. S6). If so, the concentration of *trans*-azo moieties at different irradiation times can be calculated, thus f_{philic} can be obtained. Nevertheless, we failed due to the lagged morphological evolution at the macroscopic scale, as compared with the *trans-cis* isomerization at the molecular level.

When the irradiation time of UV is prolonged to 30 min, the micelles almost disappear and particles with an irregular shape are formed (Fig. 8e). At the same time, the size of the aggregates after UV irradiation for 30 min is decreased from 170 nm to 130 nm (Fig. 8a). This shows that, after long time UV irradiation, most of the *trans*-azo isomers are changed into *cis*-azo ones and azo moieties will slide out from the cavity of β-CD due to the size mismatch between the host and guest. As a result, the PMMAZO block recovers its insoluble characteristic and the PLLA-*b*-PMMAZO forms completely insoluble aggregates. Possibly due to the presence of nearby β-CD,[45] the aggregates can stably suspend in water for a short time and don't precipitate from the solution.

On the other hand, the subsequent irradiation with 450 nm visible light for 30 min can lead to recovery of the micellar size and shape before UV irradiation (Fig. 8a and 8f). This shows that, not only the *trans*-*cis* photo-isomerization of the azo moiety but also the resulting morphological transition of PLLA-*b*-PMMAZO/β-CD complex micelles is reversible. As a result, we can switch the self-assembly morphology of the PLLA-*b*-PMMAZO/β-CD complexes simply by irradiation of UV light for different times Similar result is obtained for the $PLLA_{92}$-*b*-$PMMAZO_{26}$/β-CD complex, which is supplied in Fig. S7 of supplementary information.

We also examined the reassembly rate of the disassociated aggregates under visible light by DLS, and the variation of the aggregate size with irradiation time of visible light is shown in Fig. 9. One can see that the size of the aggregates increases quickly in the initial period, and after 3 min the size levels off about 170 nm, which is similar to the size of the vesicles before UV irradiation. This process is driven by the *cis*-*trans* isomerization under visible light, through which the host-guest interaction is recognized again. This shows that the reassembly of the disassociated aggregates can be completed within 3 min upon irradiation of visible light. As compared with the photo-isomerization rate of the azo groups (Fig. S5), the reassembly rate of the aggregates is evidently slower. This difference is understandable, since there are intermediate processes, such as re-association between *trans*-isomers with β-CD, and reassembly among different polymer chains, when the effect of the structural change of the azo groups is amplified and transferred to the inter-molecules.

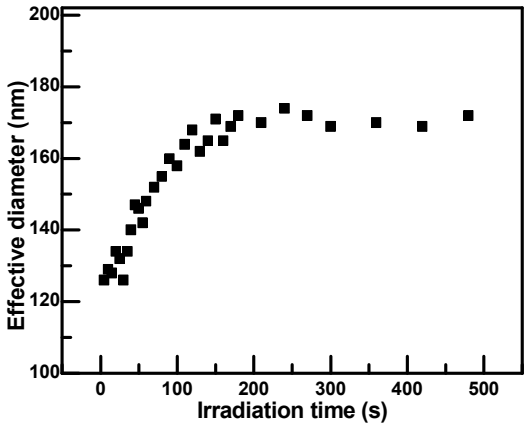

Fig. 9. Variation of the aggregate size of $PLLA_{17}$-*b*-$PMMAZO_{26}$ at β-CD/azo=1 with irradiation time of visible light.

Conclusions

A series of double hydrophobic PLLA-*b*-PMMAZO BCPs with different compositions were successfully prepared via ATRP and ring opening polymerization. The hydrophobic BCPs can self-assemble into vesicles, spherical micelles and entrapped vesicles in aqueous solution, with the aid of host-guest inclusion complexation between the azo groups and β-CD. These morphologies can be regulated by the PLLA block length, micelle concentration, β-CD/azo ratio and UV irradiation time, through which the hydrophilic/hydrophobic balance is changed. Moreover, the micelles can be reversibly disassembled and reassembled by alternative UV and visible light irradiation, which results from the reversible *trans*-*cis* isomerization of the azo moieties. In addition, the inhomogeneous complexation between the azo groups and β-CD leads to incorporation of the less complexed PMMAZO into the micellar core, thus microphase separation occurs due to the incompatibility between the less complexed PMMAZO and the hydrophobic PLLA blocks.

Acknowledgements

This work was supported by National Natural Science Foundation of China (21274130).

Notes and references

MOE Key Laboratory of Macromolecular Synthesis and Functionalization, Department of Polymer Science & Engineering, Zhejiang University, Hangzhou 310027, China.

*corresponding author: xujt@zju.edu.cn

Electronic Supplementary Information (ESI) available: synthesis of 2-HBMP; ^{1}H NMR of 2-HBMP; TEM images of $PLLA_{44}$-*b*-$PMMAZO_{26}$/β-CD complex at β-CD/azo=1 without and with PTA staining; effect of β-CD/azo ratio on the micellar morphology of $PLLA_{92}$-*b*-$PMMAZO_{26}$/β-CD complexes; Size distribution of entrapped vesicle before and after annealing; UV/vis spectra of $PLLA_{17}$-*b*-$PMMAZO_{26}$/β-CD complex (β-CD/azo=1) at different irradiation times; The effect of UV irradiation time on absorbance at 360 nm and 450 nm; Size distribution of $PLLA_{92}$-*b*-$PMMAZO_{26}$/β-CD complex at β-CD/azo=1 before and after UV irradiation, and the after irradiation with visible light. See DOI: 10.1039/b000000x/

1 G. Riess, *Prog. Polym. Sci.*, 2003, **28**, 1107-1170.
2 W. N. He and J. T. Xu, *Prog. Polym. Sci.*, 2012, **37**, 1350-1400.
3 Y. Y. Mai and A. Eisenberg, *Chem. Soc. Rev.*, 2012, **41**, 5969-5985.
4 W. N. He, B. Zhou, J. T. Xu, B. Y. Du and Z. Q. Fan, *Macromolecules*, 2012, **45**, 9768-9778.
5 L. Wang, X. F. Yu, S. G. Yang, J. X. Zheng, R. M. Van Horn, W. B. Zhang, J. T. Xu and S. Z. D. Cheng, *Macromolecules*, 2012, **45**, 3634-3638.
6 J. X. Yang, L. Liu and J. T. Xu, *Prog. Chem.*, 2014, **26**, 1811-1820.
7 D. E. Discher and A. Eisenberg, *Science*, 2002, **297**, 967-973.
8 Q. Jin, C. Luy, J. Ji and S. Agarwal, *J. Polym. Sci., Part A: Polym. Chem.*, 2012, **50**, 451-457.
9 S. Förster, M. Zisenis, E. Wenz and M. Antonietti, *J. Chem. Phys.*, 1996, **104**, 9956-9970.
10 S. Förster and M. Antonietti, *Adv. Mater.*, 1998, **10**, 195-217.
11 Z. L. Zhou, Z. B. Li, Y. Ren, M. A. Hillmyer and T. P. Lodge, *J. Am. Chem. Soc.*, 2003, **125**, 10182-10183.
12 R. C. Hayward and D. J. Pochan, *Macromolecules*, 2010, **43**, 3577-3584.
13 W. D. He, X. L. Sun, W. M. Wan and C. Y. Pan, *Macromolecules*, 2011, **44**, 3358-3365.
14 H. Shen and A. Eisenberg, *J. Phys. Chem. B*, 1999, **103**, 9473-9487.
15 S. Jain and F. S. Bates, *Macromolecules*, 2004, **37**, 1511-1523.
16 J. Bang, S. Jain, Z. Li, T. P. Lodge, J. S. Pedersen, E. Kesselman and Y. Talmon, *Macromolecules*, 2006, **39**, 1199-1208.
17 J. X. Yang, W. N. He, J. T. Xu, B. Y. Du and Z. Q. Fan, *Chin. J. Polym. Sci.*, 2014, **32**, 1128-1138.

18 N. Koumura, R. W. J. Zijlstra, R. A. van Delden, N. Harada and B. L. Feringa, *Nature*, 1999, **401**, 152-155.
19 D. Cao, M. Amelia, L. M. Klivansky, G. Koshkakaryan, S. I. Khan, M. Semeraro, S. Silvi, M. Venturi, A. Credi and Y. Liu, *J. Am. Chem. Soc.*, 2009, **132**, 1110-1122.
20 C. Y. Ang, S. Y. Tan, X. L. Wang, Q. Zhang, M. Khan, L. Bai, S. Tamil Selvan, X. Ma, L. L. Zhu, K. T. Nguyen, N. S. Tan and Y. L. Zhao, *J. Mater. Chem. B*, 2014, **2**, 1879-1890.
21 X. X. Ke, L. Wang, J. T. Xu, B. Y. Du, Y. F. Tu and Z. Q. Fan, *Soft Matter*, 2014, **10**, 5201-5211.
22 I. Tomatsu, A. Hashidzume and A. Harada, *J. Am. Chem. Soc.*, 2006, **128**, 2226-2227.
23 H. Jin, Y. L. Zheng, Y. Liu, H. X. Cheng, Y. F. Zhou and D. Y. Yan, *Angew. Chem. Int. Ed.*, 2011, **50**, 10352-10356.
24 H. Jiang, X. Chen, X. J. Pan, G. Zou and Q. J. Zhang, *Macromol. Rapid Commun.*, 2012, **33**, 773-778.
25 H. F. Yu, T. Iyoda and T. Ikeda, *J. Am. Chem. Soc.*, 2006, **128**, 11010-11011.
26 T. Seki, *Macromol. Rapid Commun.*, 2014, **35**, 271-290.
27 Y. Yan, H. B. Wang, B. Li, G. G. Hou, Z. D. Yin, L. X. Wu and V. W. W. Yam, *Angew. Chem. Int. Ed.*, 2010, **49**, 9233-9236.
28 Z. Z. Tong, J. Q. Xue, R. Y. Wang, J. Huang, J. T. Xu and Z. Q. Fan, *RSC Adv.*, 2015, **5**, 4030-4040.
29 D. R. Wang, G. Ye, Y. Zhu and X. G. Wang, *Macromolecules*, 2009, **42**, 2651-2657.
30 G. Wang, X. Tong and Y. Zhao, *Macromolecules*, 2004, **37**, 8911-8917.
31 X. Tong, G. Wang, A. Soldera and Y. Zhao, *J. Phys. Chem. B*, 2005, **109**, 20281-20287.
32 B. Yan, X. Tong, P. Ayotte and Y. Zhao, *Soft Matter*, 2011, **7**, 10001-10009.
33 W. Su, Y. H. Luo, Q. Yan, S. Wu, K. Han, Q. J. Zhang, Y. Q. Gu and Y. M. Li, *Macromol. Rapid Commun.*, 2007, **28**, 1251-1256.
34 W. Q. Sun, X. H. He, C. Y. Gao, X. J. Liao, M. R. Xie, S. L. Lin and D. Y. Yan, *Polym. Chem.*, 2013, **4**, 1939-1949.
35 D. R. Wang and X. G. Wang, *Prog. Polym. Sci.*, 2013, **38**, 271-301.
36 G. Y. Shen, G. S. Xue, J. Cai, G. Zou, Y. M. Li and Q. J. Zhang, *Soft Matter*, 2013, **9**, 2512-2517.
37 M. H. Li and P. Keller, *Soft Matter*, 2009, **5**, 927-937.
38 E. Mabrouk, D. Cuvelier, F. Brochard-Wyart, P. Nassoy and M. H. Li, *Proc. Natl. Acad. Sci. USA*, 2009, **106**, 7294-7298.
39 L. Jia and M. H. Li, *Liq. Cryst.*, 2013, **41**, 368-384.
40 X. J. Liao, G. S. Chen, X. X. Liu, W. X. Chen, F. E. Chen and M. Jiang, *Angew. Chem. Int. Ed.*, 2010, **49**, 4409-4413.
41 Y. P. Wang, M. Zhang, C. Moers, S. L. Chen, H. P. Xu, Z. Q. Wang, X. Zhang and Z. B. Li, *Polymer*, 2009, **50**, 4821-4828.
42 J. Zou, B. Guan, X. J. Liao, M. Jiang and F. G. Tao, *Macromolecules*, 2009, **42**, 7465-7473.
43 X. Mei, S. Yang, D. Y. Chen, N. J. Li, H. Li, Q. F. Xu, J. F. Ge and J. M. Lu, *Chem. Commun.*, 2012, **48**, 10010-10012.
44 G. Liu, W. Liu and C. M. Dong, *Polym. Chem.*, 2013, **4**, 3431-3443.
45 S. H. Wang, Q. X. Shen, M. H. Nawaz and W. A. Zhang, *Polym. Chem.*, 2013, **4**, 2151-2157.
46 Y. Guan, H. B. Zhao, L. X. Yu, S. C. Chen and Y. Z. Wang, *RSC Adv.*, 2014, **4**, 4955-4959.
47 X. P. Qiu, E. V. Korchagina, J. Rolland and F. M. Winnik, *Polym. Chem.*, 2014, **5**, 3656-3665.
48 M. Lahav, K. T. Ranjit, E. Katz and I. Willner, *Chem. Commun.*, 1997, **33**, 259-260.
49 Q. Jin, G. Y. Liu, X. S. Liu and J. Ji, *Soft Matter*, 2010, **6**, 5589-5595.
50 J. Z. Li, Z. Zhou, L. Ma, G. X. Chen and Q. F. Li, *Macromolecules*, 2014, **47**, 5739-5748.
51 H. Ringsdorf and H. W. Schmidt, *Makromol. Chem.*, 1984, **185**, 1327-1334.
52 J. Zou, F. G. Tao and M. Jiang, *Langmuir*, 2007, **23**, 12791-12794.
53 Y. Nagasaki, T. Okada, C. Scholz, M. Iijima, M. Kato and K. Kataoka, *Macromolecules*, 1998, **31**, 1473-1479.
54 N. Petzetakis, A. P. Dove and R. K. O'Reilly, *Chem. Sci.*, 2011, **2**, 955-960.
55 J. Yang, R. Piñol, F. Gubellini, D. Lévy, P. A. Albouy, P. Keller and M. H. Li, *Langmuir*, 2006, **22**, 7907-7911.
56 P. D. Petrov, M. Drechsler and A. H. E. Müller, *J. Phys. Chem. B*, 2009, **113**, 4218-4225.
57 N. V. Salim, N. Hameed, T. L. Hanley, L. J. Waddington, P. G. Hartley and Q. P. Guo, *Langmuir*, 2013, **29**, 9240-9248.
58 A. C. Shi and B. H. Li, *Soft Matter*, 2013, **9**, 1398-1413.
59 R. Weberskirch, J. Preuschen, H. W. Spiess and O. Nuyken, *Macromol. Chem. Phys.*, 2000, **201**, 995-1007.
60 Z. Li, E. Kesselman, Y. Talmon, M. A. Hillmyer and T. P. Lodge, *Science*, 2004, **306**, 98-101.
61 J. F. Lutz and A. Laschewsky, *Macromol. Chem. Phys.*, 2005, **206**, 813-817.
62 H. Cui, Z. Chen, S. Zhong, K. L. Wooley and D. J. Pochan, *Science*, 2007, **317**, 647-650.
63 A. Laschewsky, *Curr. Opin. Colloid Interface Sci.*, 2003, **8**, 274-281.
64 Z. H. Ju and J. P. He, *Chem. Commun.*, 2014, **50**, 8480-8483.

Table of Contents Entry

Regulation of self-assembly morphology of azobenzene-bearing double hydrophobic block copolymers in aqueous solution by shifting the dynamic host-guest complexation

Zai-Zai Tong, Rui-Yang Wang, Jie Huang, Jun-Ting Xu,* Zhi-Qiang Fan

MOE Key Laboratory of Macromolecular Synthesis and Functionalization, Department of Polymer Science & Engineering, Zhejiang University, Hangzhou 310027, China